LASER INTERFEROMETER GRAVITATIONAL WAVE OBSERVATORY
- LIGO -
CALIFORNIA INSTITUTE OF TECHNOLOGY
MASSACHUSETTS INSTITUTE OF TECHNOLOGY

Technical Note	**LIGO-T22xxxxx–**	2022/06/11

Emissivity Engineering for Radiative CryoCooling

Hiya Gada

California Institute of Technology
LIGO Project, MS 18-34
Pasadena, CA 91125
Phone (626) 395-2129
Fax (626) 304-9834
E-mail: info@ligo.caltech.edu

Massachusetts Institute of Technology
LIGO Project, Room NW22-295
Cambridge, MA 02139
Phone (617) 253-4824
Fax (617) 253-7014
E-mail: info@ligo.mit.edu

LIGO Hanford Observatory
Route 10, Mile Marker 2
Richland, WA 99352
Phone (509) 372-8106
Fax (509) 372-8137
E-mail: info@ligo.caltech.edu

LIGO Livingston Observatory
19100 LIGO Lane
Livingston, LA 70754
Phone (225) 686-3100
Fax (225) 686-7189
E-mail: info@ligo.caltech.edu

http://www.ligo.caltech.edu/

Contents

1 Introduction

The Laser Interferometer Gravitational-Wave Observatory (LIGO) measures gravitational waves and is one of the pioneering instruments which help detect black holes and neutron star mergers. The instrument, or more accurately, the suspended mirrors used, is highly susceptible to vibration noise. The third-generation upgrade, LIGO Voyager, is planned to improve the sensitivity by an additional factor of two and halve the low-frequency cutoff to 10 Hz by reducing quantum radiation pressure and shot noise, mirror thermal noise, mirror suspension thermal noise, and Newtonian gravity noise. The thermal vibrations (or thermal noise) are nullified by installing a cryogenic cooling facility which radiatively cools the silicon test masses to 123 K.

1.1 Background

Constancio et al. [1] theorized that the silicon test masses would require a high thermal emissivity coating to increase the radiative coupling to its cold environment and effectively dissipate the absorbed laser power. To this end, we wish to determine the emissivities of various black coatings as a function of temperature and subsequently use the best emissivity material for the Mariner (Voyager prototype) upgrade at the Caltech 40m Lab. This is done by obtaining cool-down curves in a cryostat designed specifically for the purpose of emissivity measurement. Using a simplified heat transfer model, the emissivity and corresponding propagated uncertainty is extracted from the cool-down temperature data.

1.2 Motivation

Running the experiment and obtaining the cool-down data is expensive and time-consuming, with a time constant of several days. It becomes infeasible to run the experiments multiple times and find the expected value of the emissivity. We thus run simulations prior to the experiment and find the optimal experimental configuration and excitation, which gives us emissivity with the least uncertainty, using Error Propagation and Fisher Information Matrix analysis. The optimal configuration and excitation input obtained will then be used in the experiment to get a close to accurate measurement of emissivity.

The lab's ongoing work includes making design changes to the cryostat, which would minimize heat leaks into the system. It would allow the test mass to cool down to 123 K quickly and reduce the thermal noise injected into the system to get a less uncertain cool-down output. My project would complement this effort by theoretically determining which design parameters contribute the most to the uncertainty in emissivity and even suggest changes in their values for future design upgrades of the cryostat. It would also corroborate the design changes already made and recommend what optimal excitation should be given to make the system robust to noise.

Further the same optimal experimental configuration obtained as a result of this project can be used for emissivity tests of many key coating materials for the LIGO Voyager upgrade.

2 The Cryostat

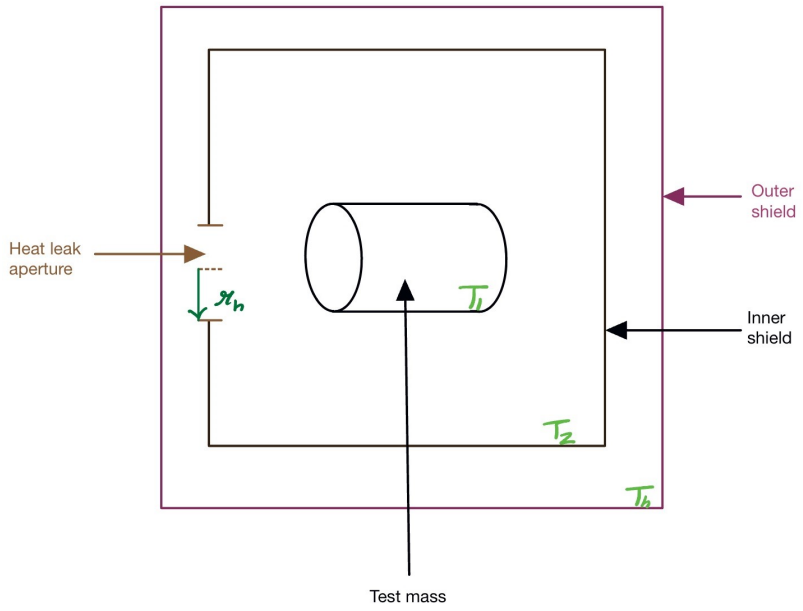

Figure 1: Caption

Figure 1 shows a simplified system diagram of the cryostat. The notation used in this report is as follows,

T_1	Test mass temperature
T_2	Inner shield temperature
T_h	Outer shield temperature
ϵ_1	Test mass emissivity
ϵ_2	Inner shield emissivity
ϵ_h	Outer shield emissivity
A_h	Total area of heat leak from the inner shield to the outer shield
r_h	Effective radius of the heat leak area
$F_{1\to h}$	Geometric view factor from the test mass to the heat leak area
A_1	Test mass surface area
A_2	Inner shield surface area
C_p	Specific heat of test mass
m	Mass of silicon test mass

2.1 Heat Model

Using radiative heat transfer equations as formulated in [2] and keeping geometric view factors in mind, we get the following simplified model of our system,

$$mC_p\frac{dT_1}{dt} = \sigma A_1\left[\frac{T_2^4 - T_1^4}{\frac{1}{\epsilon_1} + \frac{A_1}{A_2}\left(\frac{1}{\epsilon_2} - 1\right)} + \frac{T_h^4 - T_1^4}{\frac{1}{\epsilon_1} + \frac{A_1}{A_h}\left(\frac{1}{\epsilon_h} - 1\right) + \frac{1}{F_{1\to h}} - 1}\right], \tag{1}$$

where we assume that that the geometric factor from the test mass to the inner shield $F_{1\to 2} \approx 1$. The first term corresponds to the cooling term by the cold inner shield, while the second term corresponds to the heating term due to the heat leaks.

For our preliminary analysis we will consider only the steady state region of the cool-down curve. Thus, the ϵ_1, ϵ_2, ϵ_h, T_2 and T_h can be taken as constant. Moreover, it is experimentally observed that T_h realises steady state around 200 K almost every time. T_1 is the output, and $\bar{\theta} = \{\epsilon_1, \epsilon_2, \epsilon_h, r_h\}$ denotes the parameter vector for our system.

Note that the parameters A_h and $F_{1\to h}$ are combined in one parameter that is r_h. It gives us the radius of the effective circular hole causing the heat leak. Knowing r_h one can find out the corresponding A_h and $F_{1\to h}$.

3 Error Propagation

3.1 Theory

To understand quantitatively the effect of other parameters on ϵ_1, we perform error propagation analysis. At steady state, we can get a function of ϵ_1 in terms of other parameters.

$$\epsilon_1 = \frac{T_2^4 + T_h^4 - 2T_1^4}{(T_1^4 - T_h^4)\frac{A_1}{A_2}\left(\frac{1}{\epsilon_2} - 1\right) + (T_1^4 - T_2^4)\frac{A_1}{A_h}\left(\frac{1}{\epsilon_h} + \frac{1}{F_{1\to h}} - 1\right)}. \tag{2}$$

For parameters $\bar{\theta} = \{\epsilon_1, \epsilon_2, \epsilon_h, r_h\} = \{\bar{\theta}_i\}$ for $i = \{1, 2, 3, 4\}$, the variance of the parameters can be related by the following equation,

$$\sigma_{\epsilon_1}^2 = \sum_{i=2}^{4}\left(\frac{\partial\epsilon_1}{\partial\bar{\theta}_i}\right)^2\sigma_{\bar{\theta}_i}. \tag{3}$$

This equation is only applicable when the parameters $\{\epsilon_2, \epsilon_h, r_h\}$ are uncorrelated to each other. A more general relation for correlated variables as given in [3] is,

$$\sigma_{\epsilon_1}^2 = \mathbf{g}^\top\mathbf{V}\mathbf{g}, \tag{4}$$

in which the variance-covariance matrix is $\mathbf{V}$, with the i^{th} element in the vector $\mathbf{g}$ being $\frac{\partial\epsilon_1}{\partial\bar{\theta}_i}$. In fact equation (3) is just obtained by keeping $\mathbf{V}$ a diagonal matrix.

3.2 Simulation Results

We assume that our parameters are uncorrelated and use equation (3) to analyse some trends. We use the notation $\Delta\epsilon_1$ and σ_{ϵ_1} interchangeably.

The differentials are calculated at some estimate of the parameters. We take $T_h = 200K$, $T_2 = 100K$ and use the heat model (1) to find steady state value of T_1. The variance of the emissivities ϵ_2 and ϵ_h are taken to be constant and equal to 0.05. The variance of r_h is taken to be 0.01m. The trends of uncertainty in ϵ_1 as a function of other parameters are shown in figures 2, 4 and 3.

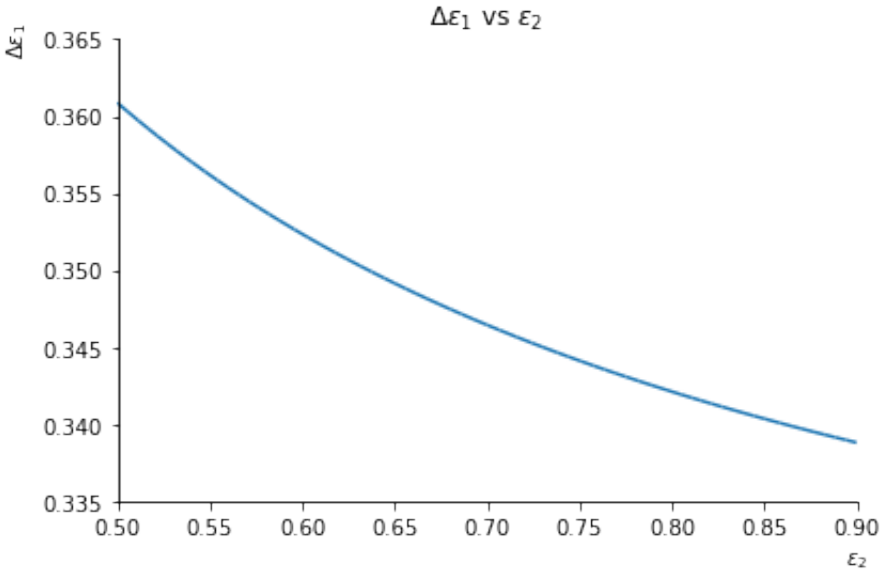

Figure 2: Variation in uncertainty of ϵ_1 with ϵ_2

3.3 Analysis and Cryostat Design Changes

In figure 2, we see that uncertainty in ϵ_1 decreases as ϵ_2 increases. The blacker the surface of the inner shield, the more certain will our measurement of ϵ_1 be. It will also increase coupling between the test mass and the inner shield, resulting in a more rapid cool-down of the test mass to steady-state conditions. To this effect, we blackened the inner surface of the inner shield and the cryostat's aluminium foil lid with an Aquadag coating.

In figure 3 we see that the uncertainty in ϵ_1 attains a minimum for a particular value of ϵ_h. ϵ_h can roughly be considered the emissivity of the outer shield, which is made of aluminium. The emissivity of aluminium is not known very accurately in literature for low-temperature values. However, we can still try to minimize our uncertainty by changing ϵ_h and getting close to the minima of $\Delta\epsilon_1$.

In figure 4, the uncertainty in ϵ_1 increases with r_h, which intuitively makes sense. The heat leaks add noise to the system, and we also do not have an accurate analytical model. The plot recommends we close up the apertures in our system, thus effectively reducing r_h. We used aluminium sheet bits to close these apertures, leaving only two open, one for the RTD

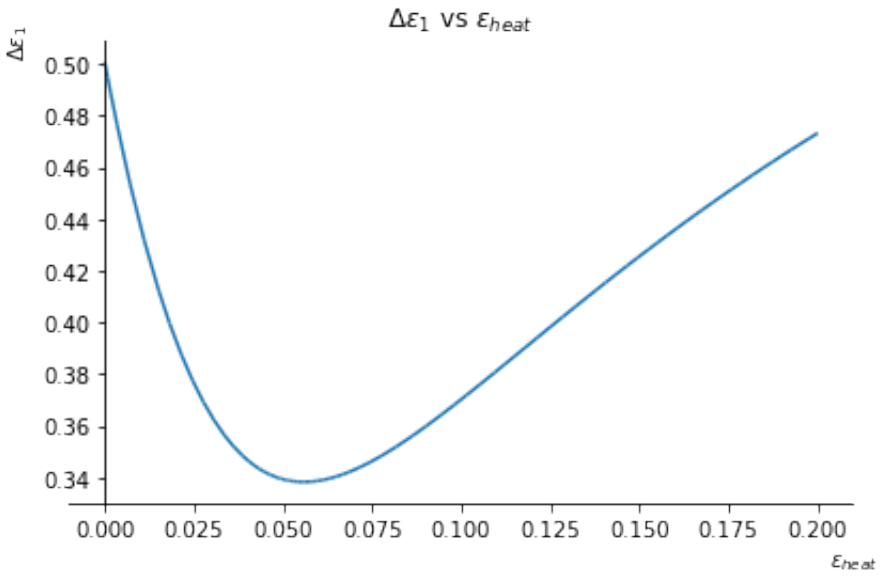

Figure 3: Variation in uncertainty of ϵ_1 with ϵ_h

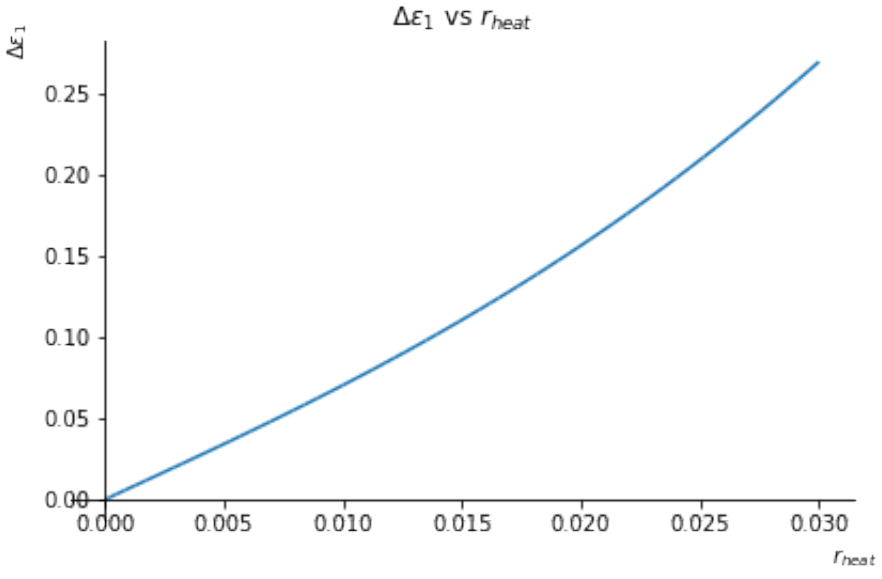

Figure 4: Variation in uncertainty of ϵ_1 with r_h

sensors and one for the cold copper bar (which is used to cool the cold plate attached to the inner shield walls). We further try to block these two apertures as much as possible using aluminium foil.

4 Fisher Information Matrix

4.1 Theory

Assuming that the measurement noise as Gaussian, the Fisher matrix is constructed from the likelihood function with the objective of maximising the curvature (or minimising uncertainty in output) as derived in [4]. The output measurement,

$$y_\alpha = H_\alpha x_\alpha + n_\alpha; \quad \alpha = 1, 2, \cdots, N,$$

where H_α is the system model and x_α is the input. The Fisher Matrix is given by,

$$\begin{aligned}
\mathcal{F}_{ij} &= -\left.\frac{\partial^2[\ln \mathcal{L}]}{\partial\theta_i\theta_j}\right|_{\bar{\theta}}, \\
&= \sum_\alpha \frac{1}{|n_\alpha|^2}\,\mathrm{Re}\left[\frac{\partial\hat{y}_\alpha^*}{\partial\theta_i}\frac{\partial\hat{y}_\alpha}{\partial\theta_j}\right]\Bigg|_{\bar{\theta}}, \\
&= \sum_\alpha \frac{1}{\sigma_{H_\alpha}^2}\,\mathrm{Re}\left[\frac{\partial\hat{H}_\alpha^*}{\partial\theta_i}\frac{\partial\hat{H}_\alpha}{\partial\theta_j}\right]\Bigg|_{\bar{\theta}},
\end{aligned}$$

where $\hat{H}_\alpha$ denotes the estimate of the system model, which is dependant on the parameters $\bar{\theta}$ we choose. The Cramer-Rao bound gives a lower limit on the covariance matrix $\mathcal{C}$ and relates it to the Fisher Matrix. For unbiased parameters,

$$\mathcal{C} \geq \mathcal{F}^{-1},$$

where the inequality is understood to be element-wise. Our objective is to select those parameters which maximize the Fisher information (and thus minimize variance-covariance). We do this by either maximising the determinant of the Fisher Matrix or minimising the variance of ϵ_1 as that is the parameter of major interest.

4.2 Transfer function

Consider additional power input by a lamp shining on our test mass and modifying equation (1) we get,

$$mC_p\frac{dT_1}{dt} = \sigma A_1\left[\frac{T_2^4 - T_1^4}{\frac{1}{\epsilon_1} + \frac{A_1}{A_2}\left(\frac{1}{\epsilon_2} - 1\right)} + \frac{T_h^4 - T_1^4}{\frac{1}{\epsilon_1} + \frac{A_1}{A_h}\left(\frac{1}{\epsilon_h} - 1\right) + \frac{1}{F_{1\to h}} - 1}\right] + P(t),$$

where $P(t)$ is the heat power input as a function of time. We will linearize this system about the steady state equilibrium and make a bode plot.

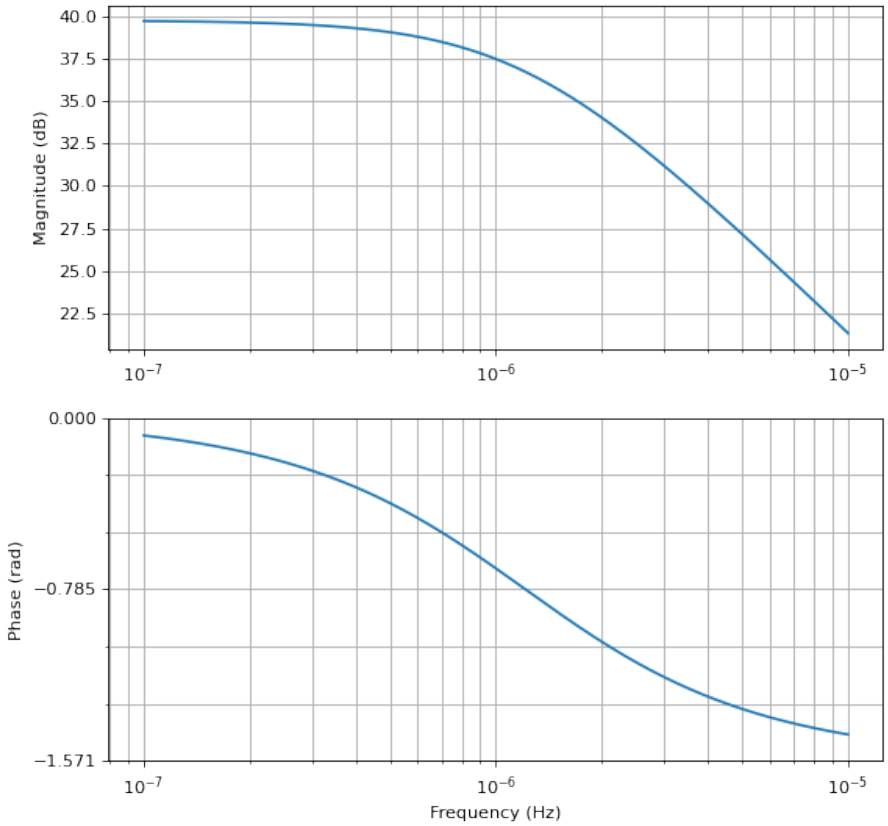

Figure 5: Bode plot of the heat model transfer function

As we can see the cross-over frequency is very low, around 10^{-6} Hz. This means that any effective excitation to the system would be at less than 10^{-6} Hz. This means that the time constant of that signal would be about 5 days which is infeasible as we want our tests to be done under 12 hours if possible. Thus, we can conclude that frequency domain analysis of Fisher matrix may not give us a feasible input power signal. We verify this in the next section.

4.3 Frequency Domain Analysis

We take one parameter at a time with ϵ_1 and analyse its 2×2 Fisher matrix for one excitation frequency. We add our prior information as well, to get the resultant Fisher matrix.

Without priors, the matrices end up giving 0 information ($\det(\mathcal{F}) = 0$) for one excitation frequency. This is because we cannot extract two parameters by making only one measurement. We need at least two measurements and hence two excitation frequencies. Thus, we add the information from the priors on all parameters except ϵ_1 to the corresponding diagonal terms to get the result fisher matrix. This gives a $\det(\mathcal{F}) \neq 0$ and we can proceed with our analysis.

Analytically, the maxima of $\det(\mathcal{F})$ turns out to be at 0 Hz frequency. Figure 6 is plotted for the Fisher Matrix of ϵ_1 and ϵ_2. A similar trend is observed for other combinations.

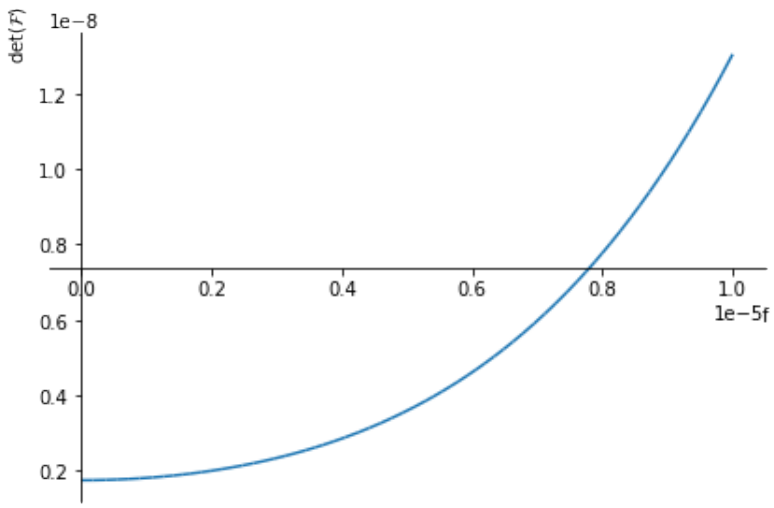

Figure 6: Plot of det($\mathcal{F}$) vs frequency

We realise that frequency domain analysis is not particularly helpful for single frequency excitation as the optimal frequency comes out to be a constant values signal in time domain. This is already the case for our current system where the cold head cools the system at a constant power.

4.4 Time Domain Analysis

We now try to get some useful information using time domain analysis taking our model y_α to be our T_1 temperature measurement. If we take power to be our input signal and try to find the best input to give which could maximise our Fisher Matrix, we realise that the input does not come into the Fisher Matrix at all. This means that the control input does not affect the covariance in the time domain.

Another, and hopefully more promising, way to approach the time domain analysis is to create a new parameter, say T_1^0. Assume our system has cooled down and is at steady state. We install a heat lamp used to heat our test mass which is switched on during steady state. The duration and power of the heating will be determined by what temperature T_1^0 we want the test mass to reach. We can develop another Fisher matrix which captures this parameter and optimise the information.

5 Future Work

With the data obtained from the cryostat with the latest design changes, I intend to work on curve fitting the data to find the parameters and experimental configuration for our simplified heat model (1).

I will also continue working on the time-domain analysis of the Fisher Matrix in the case where a step heat excitation is provided for an interval. The parameters we control is how much and how long we heat the test mass. This is done so that we obtain a cool-down curve

for the test mass when all the other parts in the cryostat are at steady state temperatures. This will allow us to study a cool-down curve at steady states where we possibly may get more certain measurements of emissivity.

References

[1]M. Constancio Jr, R. X. Adhikari, O. D. Aguiar, K. Arai, A. Markowitz, M. A. Okada, and C. C. Wipf, "Silicon emissivity as a function of temperature", International Journal of Heat and Mass Transfer **157**, 119863 (2020).

[2]Y. A. Çengel, *Heat transfer: a practical approach*, McGraw-Hill series in mechanical engineering (McGraw-Hill, 2003) Chap. 12.

[3]J. Tellinghuisen, "Statistical error propagation", The Journal of Physical Chemistry A **105**, 3917–3921 (2001).

[4]E. D. Hall, "Fisher matrix methods for transfer function measurement", ligo (2015).

[5]D. Wittman, "Fisher matrix for beginners", Technical report, UC Davis.

[6]R. Pintelon and J. Schoukens, *System identification: a frequency domain approach* (John Wiley & Sons, 2012).

[7]R. X. Adhikari, K. Arai, A. F. Brooks, C. Wipf, O. Aguiar, P. Altin, B. Barr, L. Barsotti, R. Bassiri, A. Bell, G. Billingsley, R. Birney, D. Blair, E. Bonilla, J. Briggs, D. D. Brown, R. Byer, H. Cao, M. Constancio, S. Cooper, T. Corbitt, D. Coyne, A. Cumming, E. Daw, R. deRosa, G. Eddolls, J. Eichholz, M. Evans, M. Fejer, E. C. Ferreira, A. Freise, V. V. Frolov, S. Gras, A. Green, H. Grote, E. Gustafson, E. D. Hall, G. Hammond, J. Harms, G. Harry, K. Haughian, D. Heinert, M. Heintze, F. Hellman, J. Hennig, M. Hennig, S. Hild, J. Hough, W. Johnson, B. Kamai, D. Kapasi, K. Komori, D. Koptsov, M. Korobko, W. Z. Korth, K. Kuns, B. Lantz, S. Leavey, F. Magana-Sandoval, G. Mansell, A. Markosyan, A. Markowitz, I. Martin, R. Martin, D. Martynov, D. E. McClelland, G. McGhee, T. McRae, J. Mills, V. Mitrofanov, M. Molina-Ruiz, C. Mow-Lowry, J. Munch, P. Murray, S. Ng, M. A. Okada, D. J. Ottaway, L. Prokhorov, V. Quetschke, S. Reid, D. Reitze, J. Richardson, R. Robie, I. Romero-Shaw, R. Route, S. Rowan, R. Schnabel, M. Schneewind, F. Seifert, D. Shaddock, B. Shapiro, D. Shoemaker, A. S. Silva, B. Slagmolen, J. Smith, N. Smith, J. Steinlechner, K. Strain, D. Taira, S. Tait, D. Tanner, Z. Tornasi, C. Torrie, M. V. Veggel, J. Vanheijningen, P. Veitch, A. Wade, G. Wallace, R. Ward, R. Weiss, P. Wessels, B. Willke, H. Yamamoto, M. J. Yap, and C. Zhao, "A cryogenic silicon interferometer for gravitational-wave detection", Classical and Quantum Gravity **37**, 165003 (2020).